Pflugers Arch - Eur J Physiol (2004) 448: 363–375
DOI 10.1007/s00424-004-1250-0

Thomas Desplantez · Deborah Halliday · Emmanuel Dupont · Robert Weingart

Cardiac connexins Cx43 and Cx45: formation of diverse gap junction channels with diverse electrical properties

Received: 15 January 2004 / Accepted: 6 February 2004 / Published online: 27 March 2004
© Springer-Verlag 2004

Abstract HeLa cells expressing rat connexin43 (Cx43) and/or mouse Cx45 were studied with the dual voltage-clamp technique. Different types of cell pairs were established and their gap junction properties determined, i.e. the dependence of the instantaneous and steady-state conductances ($g_{j,inst}$, $g_{j,ss}$) on the transjunctional voltage (V_j) and the kinetics of inactivation of the gap junction current (I_j). Pairs of singly transfected cells showed homogeneous behaviour at both V_j polarities. Homotypic Cx43-Cx43 and Cx45-Cx45 cell pairs yielded distinct symmetrical functions $g_{j,inst}=f(V_j)$ and $g_{j,ss}=f(V_j)$. Heterotypic Cx43-Cx45 preparations exhibited asymmetric functions $g_{j,inst}=f(V_j)$ and $g_{j,ss}=f(V_j)$ suggesting that connexons Cx43 and Cx45 gate with positive and negative V_j, respectively. Preparations containing a singly (Cx43 or Cx45) or doubly (Cx43/45) transfected cell showed quasi-homogeneous behaviour at one V_j polarity and heterogeneous behaviour at the other polarity. The former yielded Boltzmann parameters intermediate between those of Cx43-Cx43, Cx45-Cx45 and Cx43-Cx45 preparations; the latter could not be explained by homotypic and heterotypic combinations of homomeric connexons. Each pair of doubly transfected cells (Cx43/Cx45) yielded unique functions $g_{j,inst}=f(V_j)$ and $g_{j,ss}=f(V_j)$. This can not be explained by combinations of homomeric connexons. We conclude that Cx43 and Cx45 form homomeric-homotypic, homomeric-heterotypic channels as well as heteromeric-homotypic and heteromeric-heterotypic channels. This has implications for the impulse propagation in specific areas of the heart.

Keywords Connexin43 · Connexin45 · Heterotypic channels · Heteromeric channels · Electrical properties

T. Desplantez · R. Weingart (✉)
Physiologisches Institut, Universität Bern,
Bühlplatz 5,
3012 Bern, Switzerland
e-mail: weingart@pyl.unibe.ch
Tel.: +41-31-6318706
Fax: +41-31-6314611

D. Halliday · E. Dupont
National Heart and Lung Institute (Imperial College London),
Royal Brompton Hospital,
Sydney Street,
London, SW3 6NP, UK

Introduction

Gap junction channels are intercellular channels that provide a pathway for direct communication between adjacent cells. They consist of transmembrane proteins called connexins. Six connexins assemble to form a hemichannel (connexon) with an aqueous pore. The docking of two connexons leads to the establishment of a gap junction channel [5]. So far, 20 different connexins, encoded by a multi-gene family, have been identified in vertebrate tissues (see [37]). Most vertebrate tissues express gap junction channels. They mediate electrical coupling between cells and enable the intercellular exchange of signalling molecules and nutrients (see [15]). These processes serve important biological functions and are operational under physiological and pathophysiological conditions [19, 24].

In many tissues, the cells express more than one type of connexin [8, 13, 18]. This offers the possibility of forming different types of connexons. As shown in Fig. 1A, co-expression of two types of connexins leads to the formation of two types of connexons, homomeric and heteromeric. In the former case, two complementary structures are possible. In the latter case, 12 different combinations are possible depending on the relative contribution of the connexins and their arrangement. As shown in Fig. 1B, hemichannel docking leads to two classes of gap junction channels, homotypic and heterotypic. For homomeric connexons, two homomeric-homotypic and one homomeric-heterotypic channels are possible. For heteromeric connexons, the number of structurally different channels increases drastically, i.e. 12 heteromer-

ic-homotypic and $14^2-(12+3)=181$ heteromeric-heterotypic channels are possible [36].

In the past, most electrophysiological studies have been performed on transfected cells or injected oocytes expressing one type of connexin. This has enabled the properties of homomeric-homotypic and homomeric-heterotypic channels to be determined (see [15]). It turned out that each type of channel exhibits its own set of properties. While these data were useful for elucidating the basic mechanisms of channel operation, they failed to explain the complex properties of gap junctions seen in cells isolated from intact tissues. However, with the properties of homomeric-homotypic and homomeric-heterotypic channels at hand, investigators set out to study more complex channels using model cells and freshly isolated cells [16, 21, 22, 23, 31].

In the heart, three main connexins have been identified, Cx40, Cx43 and Cx45. They are expressed in different areas, often co-localized in the same junction [13, 34]. The aim of this study was to examine the electrical properties of gap junction channels involving Cx43 and Cx45. Experiments were carried out on pairs of HeLa cells expressing rat Cx43 and mouse Cx45, singly transfected or co-transfected. They allow the formation of different types of gap junction channels. The parameters explored included the voltage sensitivity and the kinetics of inactivation. Preliminary results have been presented elsewhere [11].

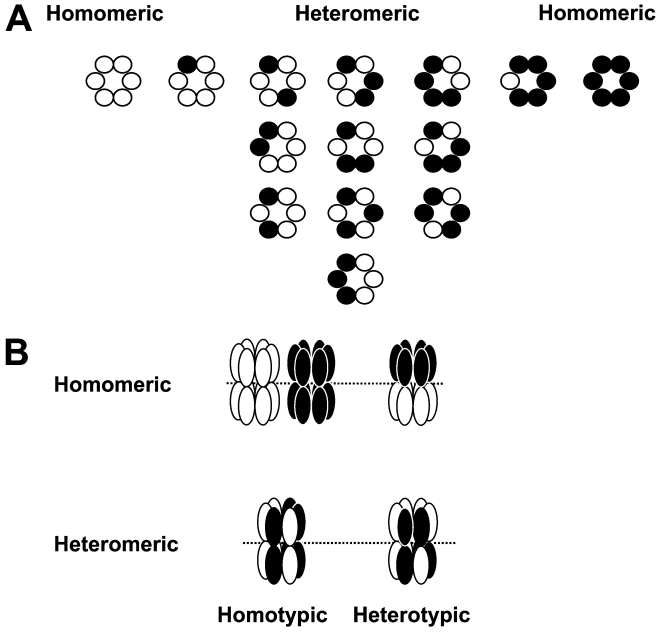

Fig. 1A, B Predicted configurations of connexons and gap junction channels for two different connexins (Cx). **A** Fourteen different connexons can be formed when two connexins are co-expressed in a cell: 2 homomeric connexons, consisting of one type of connexin, and 12 heteromeric connexons consisting of two types of connexins. **B** Diversity of gap junction channels formed after docking of two connexons. They can be homotypic when the connexons are identical (composed of one or two types of connexins) or heterotypic when the connexons are different (composed of one or two types of connexins)

Materials and methods

Cell cultures

Transfected human HeLa cells (ATCC code CCL2) expressing rat Cx43 and/or mouse Cx45 (rCx43, mCx45) were grown in DMEM supplemented with 10% FBS, 100 µg/ml streptomycin and 100 U/ml penicillin and the antibiotic used as the selection marker for transfection and clone maintenance. The DNA construct used to obtain the Cx43 transfectants generated a bi-cistronic RNA that contained Cx43, an internal ribosome entry site (IRES) and the hygromycin B resistance gene and was selected with 500 µ/ml hygromycin B (rCx43) [14]. The two other transfectants used DNA constructs with two separate transcription units, one for Cx and one for antibiotic resistance, and were grown with 1 µg/ml puromycin (mCx45) or 300 µg/ml G418 and 0.25 µg/ml puromycin (rCx43/mCx45). The cells were kept in an incubator at 37 °C (5% CO_2, 95% ambient air) and passaged weekly. To carry out experiments, the cells were seeded onto sterile glass cover-slips placed in Petri dishes. They were ready for use 1–2 days after plating. For mixed cultures, prior to plating one type of cell was labelled with a fluorescent dye (5-chloromethylfluorescein diacetate, CMFDA, 2.5 µM, 1 h; Molecular Probes, Eugene, Ore., USA).

Solutions

Experiments were performed in modified Krebs-Ringer solution (in mM): NaCl 140, KCl 4, $CaCl_2$ 2, $MgCl_2$ 1, HEPES 5 (pH 7,4), Na-pyruvate 2, glucose 5. Pipettes were filled with internal solution (in mM): K-aspartate 130, NaCl 10, $CaCl_2$ 1, MgATP 3, EGTA 10 (pCa≅8), HEPES 5 (pH 7.2).

Electrophysiological measurements

Glass cover-slips with adherent cells were transferred to a chamber placed on an inverted microscope (Diaphot-TMD, Nikon; Nippon Kogaku, Tokyo, Japan) and superfused with Krebs-Ringer solution at room temperature (22–25 °C). Patch pipettes were pulled from glass capillaries (GC150F-10; Harvard Apparatus, Edenbridge, Kent, UK) using a horizontal puller (DMZ Universal; Zeitz Instruments, Munich, Germany). When filled with solution, the pipettes had resistances of 3–6 MΩ. Electrical measurements were performed on cell pairs using a dual voltage-clamp method and whole-cell recording (manipulators: MP-285; Sutter Instruments, Novato, Calif., USA; amplifier: EPC 9/2; HEKA Electronic, Darmstadt, Germany). This method permits the membrane potential (V) of each cell to be controlled and the gap junction current (I_j) to be measured [28]. To start with, the membrane potential of both cells was clamped to the same value, $V_1=V_2=0$ mV. Thereafter, V_1 was then stepped to different levels to establish a gap junction potential V_j (V_2-V_1). The current measured from cell 1 represents the sum of two components, I_j and the membrane current of cell 1 (I_{m1}); the current measured from cell 2 corresponds to $-I_j$.

Data acquisition and analysis

Voltage and current signals were stored on a PC for off-line analysis. Current signals were Bessel-filtered (1 kHz) and digitized (3.33 kHz). Data were acquired and analysed using standard software (Pulse, Pulsfit, HEKA), curves were fitted and statistics calculated using SigmaPlot and SigmaStat (Jandel Scientific, Erkrath, Germany).

For analysis, the amplitude of I_j was determined at the beginning (instantaneous, $I_{j,inst}$) and end (steady state $I_{j,ss}$) of each V_j pulse. At large V_j, $I_{j,inst}$ was gained by extrapolation to the time $t=0$ s (onset of pulse). The respective conductances were calculated as $g_{j,inst}=$

$I_{j,inst}/V_j$ and $g_{j,ss}=I_{j,ss}/V_j$. The values of $g_{j,inst}$ were normalized with respect to g_j associated with a small test pulse applied prior to each V_j pulse. The values obtained were sampled, averaged and plotted as a function of V_j. Curves were fitted with a function derived from our gap junction model (see Eq. 29 in [35]):

$$g_{j,inst} = \frac{G_j}{e^{\frac{-V_j}{V_H\left(1+e^{V_j/V_H}\right)}} + e^{\frac{V_j}{V_H\left(1+e^{-V_j/V_H}\right)}}} \quad (1)$$

The values of $g_{j,ss}$ were normalized with respect to $g_{j,inst}$, sampled, averaged and plotted as a function of V_j. Curves were fitted with the Boltzmann equation separately applied to negative and positive V_j [29]:

$$g_{j,ss} = \frac{1 - g_{j,min}}{1 + e^{\left[A\cdot\left(V_j - V_{j,0}\right)\right]}} + g_{j,min} \quad (2)$$

where $V_{j,0}$ is the value of V_j at which $g_{j,ss}/g_{j,inst}$ is half-maximally inactivated, $g_{j,min}$ the minimum value of g_j at large V_j and z the number of unitary positive charges moving through the electric field applied.

For biphasic behaviour, as observed with homomeric-heterotypic channels, the $g_{j,ss}$ data were fitted to a modified Boltzmann equation that allowed the simultaneous fit of positive and negative polarities of V_j [6].

Modelling

The functions $g_{j,ss}=f(V_j)$, experimentally determined from Cx43-Cx43, Cx45-Cx45 and Cx43-Cx45 cell pairs, were used as reference functions to predict the behaviour of gap junctions consisting of a mixture of two kinds of channels involving homomeric-homotypic and homomeric-heterotypic channels. The calculations were performed with the equation:

$$g_{j,ss} = f(V_j) = \{p[g_{j,ss} = f(V_j)]_1\} + \{q[g_{j,ss} = f(V_j)]_2\} \quad (3)$$

The functions describing the behaviour of the reference channels, i.e. $[g_{j,ss}=f(V_j)]_1$ and $[g_{j,ss}=f(V_j)]_2$, were added considering the different weights p and q (p/q=100/0%, 75/25%, 50/50%, 25/75%, 0/100%) and orientation.

Results

Voltage dependence of g_j in Cx43-Cx43 and Cx45-Cx45 cell pairs

In the first series of experiments, we examined the properties of homomeric-homotypic channels, i.e. cell pairs expressing either Cx43 or Cx45. The purpose was to establish standards for the interpretation of more complex channels. Figure 2 illustrates the experimental procedure and the results for Cx43-Cx43 cell pairs. Figure 2A shows a scheme of the preparations emphasizing the connexin distribution and the nomenclature used; Fig. 2B shows selected current signals documenting the flow of current through the gap junction I_j elicited by a junctional voltage V_j of ±10, ±40, ±70, ±100 and ±130 mV. The larger the amplitude of V_j, the larger the associated I_j and the faster its inactivation. The records displayed in Fig. 2B and others from the same experiment were analysed to determine the amplitude of the instantaneous current $I_{j,inst}$ and the steady-state current $I_{j,ss}$. The values obtained were used to calculate the normalized conductances $g_{j,inst} = I_{j,inst}/V_j$ and $g_{j,ss} = I_{j,ss}/V_j$.

Figure 2C illustrates the results from 11 cell pairs plotting the average values of $g_{j,inst}$ and $g_{j,ss}$ as functions of V_j. The smooth curves describing the function $g_{j,inst}=f(V_j)$ correspond to the best fit of data to Eq. 1 using the following values (negative/positive V_j): G_j=1.99/2.01, V_H=−175.8/175.7 mV. Starting from a maximum of 0.99/1.0 at V_j=0 mV, $g_{j,inst}$ decreased to 0.88/0.97 at V_j=±100 mV. The smooth curves that describe the function $g_{j,ss}=f(V_j)$ represent the best fit of data to Eq. 2 using the following values (negative/positive V_j): $V_{j,0}$=−60.8/62.9 mV, $g_{j,min}$=0.26/0.25, z=−3.4/2.9. When extrapolated to

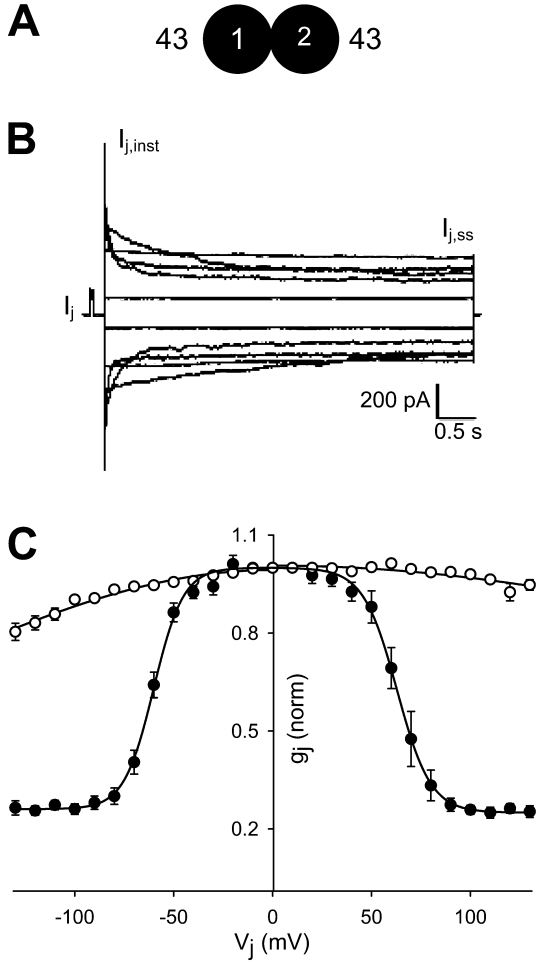

Fig. 2A–C Dependence of the gap junction conductance g_j on junctional potential V_j for homotypic Cx43-Cx43 channels. **A** Scheme of cell-pair configuration. **B** Family of junctional current signals I_j recorded at V_j=±10, ±40, ±70, ±100 and ±130 mV. Voltage pulses were applied to cell 1 (*left-hand cell*) and instantaneous ($I_{j,inst}$, start of pulse) and steady-state ($I_{j,ss}$, at end of pulse) currents were measured from cell 2 (*right-hand cell*). Depolarization of cell 1 gave rise to a negative V_j and was accompanied by a *downwards* deflection of I_j. **C** Normalized instantaneous conductance $g_{j,inst}$ (○) and steady-state conductance $g_{j,ss}$ (●), as functions of V_j. Means ±SEM. The *curves* correspond to the best fit of data to the Eqs. 1 and 2, respectively (for further explanations, see text)

V_j=0 mV, the cell pairs yielded an average $g_{j,inst}$ of 8.0 ±1.6 nS. To minimize series resistance problems, preparations with $g_{j,inst}$>11 nS were excluded from the analysis [33].

Figure 3 summarizes the results obtained for Cx45-Cx45 cell pairs. Figure 3A depicts the configuration of the preparations; Fig. 3B shows current signals elicited by the pulse protocol used for the experiments shown in Fig. 2. Distinct differences in the V_j-dependent inactivation of I_j are apparent. Figure 3C illustrates the results from 14 cell pairs plotting the average values of $g_{j,inst}$ and $g_{j,ss}$ as functions of V_j. The smooth curves describing the function $g_{j,inst}$=f(V_j) correspond to the best fit of data to Eq. 1 using the following values: G_j=1.99/2.02, V_H=−112.7/135 mV. Starting from a maximum of 0.99/1.0 at V_j=0 mV, $g_{j,inst}$ decreased to 0.76/0.82 at V_j=±100 mV. Hence, $g_{j,inst}$ of Cx45-Cx45 channels is more voltage sensitive than that of Cx43-Cx43 channels. The smooth curves describing the function $g_{j,ss}$=f(V_j) represent the best fit of data to Eq. 2 using the following values (negative/positive V_j): $V_{j,0}$= −38.9/38.5 mV; $g_{j,min}$=0.17/0.16; z=−2.5/2.7. $g_{j,ss}$ of Cx45-Cx45 channels is thus also more voltage sensitive than that of Cx43-Cx43 channels. The cell pairs analysed yielded an average $g_{j,inst}$ of 6.0±0.5 nS at V_j=0 mV. Data from preparations with $g_{j,inst}$>12 nS were discarded.

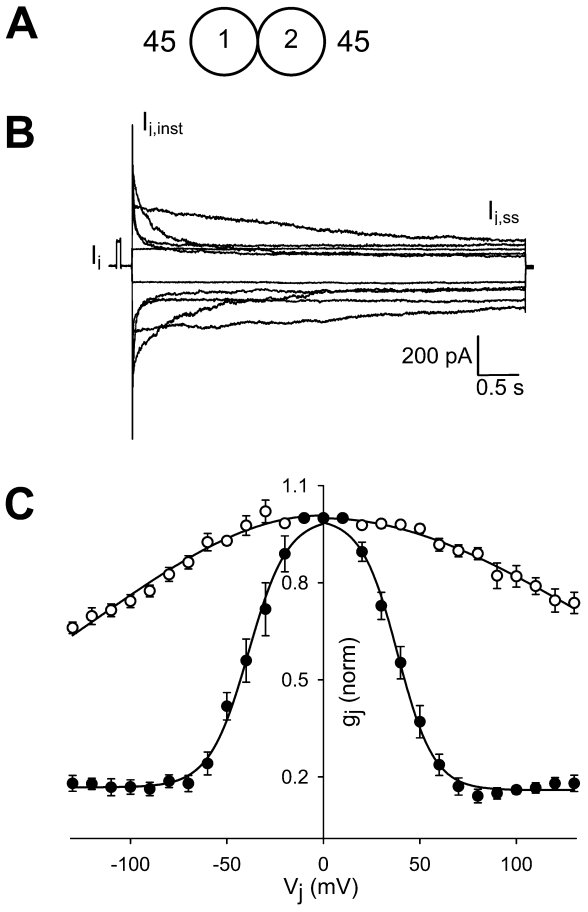

Fig. 3A–C Dependence of the gap junction conductance on junctional potential for homotypic Cx45-Cx45 channels. **A** Cell-pair configuration. **B** Superimposed records of junctional currents elicited by the pulse protocol used in Fig. 2. **C** Normalized instantaneous (○) and steady-state (●) conductances as functions of V_j. Means±SEM. The *curves* show the best fit of data to the Eqs. 1 and 2, respectively (for details, see text)

Voltage dependence of g_j in Cx43-Cx45 cell pairs

The second series of experiments explored the properties of homomeric-heterotypic channels. For this purpose, HeLa cells expressing Cx43 or Cx45 were co-cultured and mixed cell pairs selected visually (see Materials and methods). As shown in Fig. 4A, the cells expressing Cx43 and Cx45 were named cell 1 and cell 2, respectively. Figure 4B shows superimposed current signals obtained with the standard pulse protocol. Unlike Cx43-Cx43 and Cx45-Cx45 channels (Figs. 2B and 3B), the currents were asymmetrical with regard to the polarity of V_j. The inwards currents associated with depolarization of cell 1 were small and inactivated with time. In contrast, the outwards currents following hyperpolarization of cell 1 were large and diverse, i.e. some increased with time, others first increased and then decreased.

Figure 4C summarizes the results from ten experiments illustrating the relationships $g_{j,inst}$=f(V_j) and $g_{j,ss}$=f(V_j). A negative V_j prevailed when cell 1 was depolarized (the Cx43 connexon was positive, the Cx45 connexon negative); a positive V_j prevailed when cell 1 was hyperpolarized (the Cx43 connexon was negative, the Cx45 connexon positive). The functions $g_{j,inst}$=f(V_j) and $g_{j,ss}$=f(V_j) were both asymmetrical. Depolarization of cell 1 decreased $g_{j,inst}$ and $g_{j,ss}$, the former being affected more prominently. In contrast, hyperpolarization of cell 1 led to a moderate decline of $g_{j,inst}$ while $g_{j,ss}$ first increased above, and then fell below $g_{j,inst}$. The smooth curves represent the best fit of $g_{j,inst}$ and $g_{j,ss}$ to Eqs. 1 and 3, respectively. For the $g_{j,inst}$ data, curve fitting yielded the following values (negative/positive V_j): $G_{j,inst}$=1.93/2.0, V_H=−130/404 mV. Hence, starting from a maximum of 0.97/1.0 at V_j=0 mV, $g_{j,inst}$ decreased to 0.79/0.98 at V_j= ±100 mV. For $g_{j,ss}$, curve fitting yielded the following values (negative/positive V_j): $V_{j,0}$=−11.7/134.4 mV, $g_{j,min}$=0.05, $g_{j,max}$=1.41, z=−2.1/0.6. The cell pairs had an average $g_{j,inst}$ of 8.3±0.9 nS at V_j=0 mV. Data from preparations with $g_{j,inst}$>16 nS were discarded.

Voltage dependence of g_j in Cx43/Cx45-Cx43 and Cx43/45-Cx45 cell pairs

As outlined in Fig. 1B, cells that co-express two different connexins may form 181 structurally different types of channels. The following strategy was chosen to reduce this number. Cells expressing both Cx43 and Cx45 (Cx43/45) were co-cultured with cells expressing Cx43 or Cx45. This led to the formation of Cx43/45-Cx43 or Cx43/45-Cx45 cell pairs, respectively. As indicated in Figs. 5A and 6A, the co-expressing cell was named cell 1. Figure 5B shows a family of current records from a Cx43/Cx45-Cx43 cell

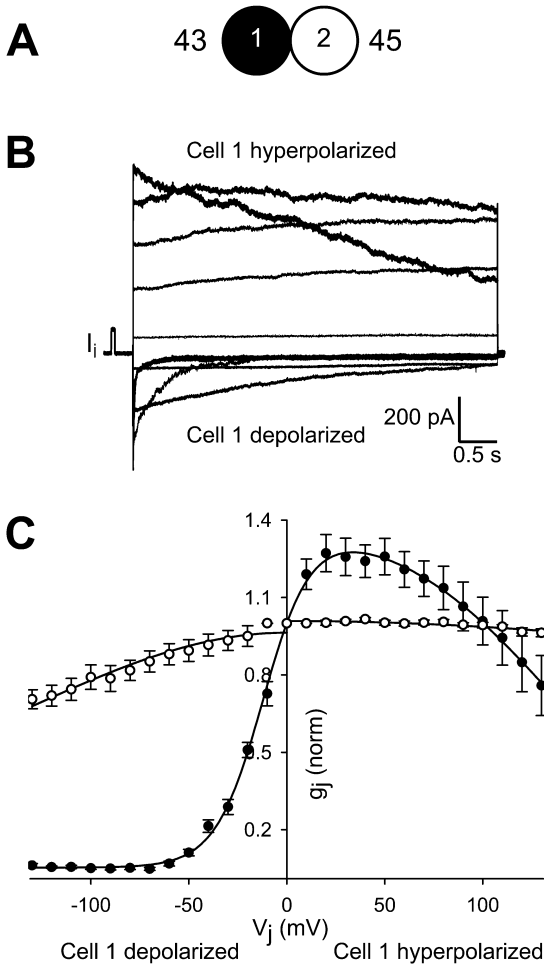

Fig. 4A–C Dependence of the gap junction conductance on junctional potential for heterotypic Cx43-Cx45 channels. **A** Cell-pair configuration. **B** Family of current records associated with the standard pulse protocol (see Fig. 2). **C** Normalized functions $g_{j,inst}=f(V_j)$ (○) and $g_{j,ss}=f(V_j)$ (●). In both cases, the V_j sensitivity is more pronounced when the cell Cx43 is made more positive, thus leading to a weak and strong rectification, respectively. The *curves* correspond to the best fit of data to the Eqs. 1 and 3 (for details, see text)

pair gained with the standard voltage protocol. The currents obtained were asymmetrical. They inactivated more rapidly and more completely when cell 1 was hyperpolarized. Figure 5C shows plots of the function $g_{j,ss}=f(V_j)$ for ten selected Cx43/45-Cx43 cell pairs (symbols indicate different preparations). The plots exhibited a distinct pattern of voltage gating. When cell 1 was hyperpolarized (the homomeric Cx43 connexons in cell 2 were positive), the function was similar in each preparation. Hence, pooling and averaging yielded a unique curve with the following Boltzmann parameters (positive V_j): $V_{j,0}=49.7\pm1.8$ mV, $g_{j,min}=0.16\pm0.03$, $z=1.5\pm0.13$. When cell 1 was depolarized (the homomeric Cx43 connexons in cell 2 were negative), the function $g_{j,ss}=f(V_j)$ was different in each preparation. Its contour varied from a transient increase to a S-shaped decrease of variable extent. Likewise, the V_j polarity giving rise to the unique function $g_{j,ss}=f(V_j)$ yielded a function $g_{j,inst}=f(V_j)$ which was similar in each cell pair (data omitted for clarity). Curve fitting of the averaged data yielded the following values (positive V_j): $G_j=2.0\pm0.005$, $V_H=160.6\pm2.10$ mV. Specifically, starting from 1.0 at $V_j=0$ mV, $g_{j,inst}$ decreased to 0.85 at $V_j=100$ mV. Similarly, the V_j polarity that led to inhomogeneous functions $g_{j,ss}=f(V_j)$ gave rise to different $g_{j,inst}$ data in each preparation (data omitted for clarity). The cell pairs included in the analysis yielded an average $g_{j,inst}$ of 11.7 ± 1.0 nS at $V_j=0$ mV ($n=28$). Preparations with $g_{j,inst}>16$ nS were discarded.

For Cx43/45-Cx45 cell pairs, the gating behaviour was different. Figure 6B shows a family of current records obtained from such a preparation. They were asymmetrical and inactivated more rapidly and more completely when cell 1 was depolarized (the homomeric Cx45 connexons in cell 2 were negative). Fig. 6C shows plots of the function

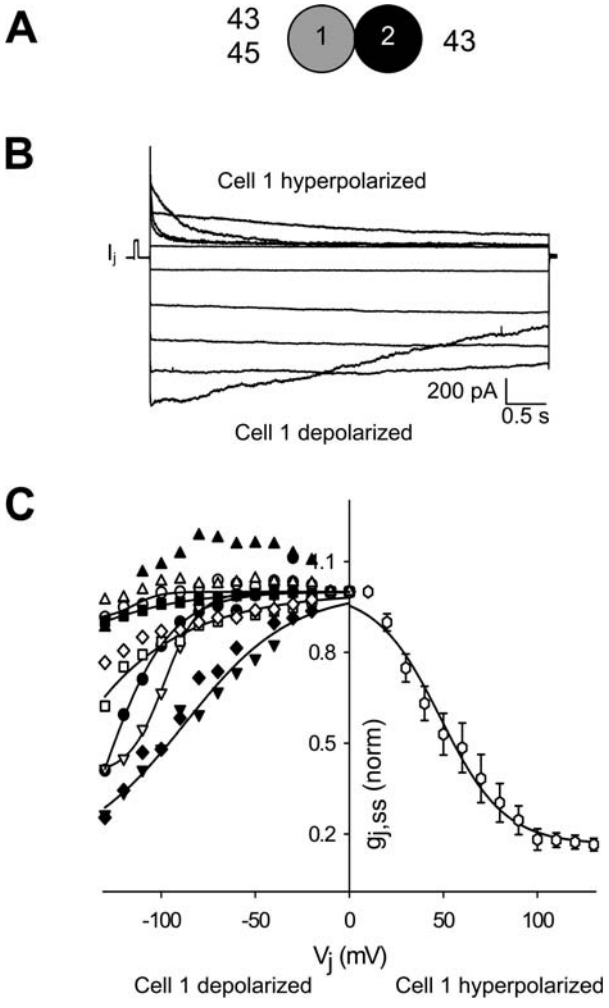

Fig. 5A–C Dependence of steady-state gap junction conductance on junctional potential of mixed-Cx43 cell pairs consisting of a co-transfected cell (Cx43/45) and a singly transfected cell (Cx43). **A** Cell-pair configuration. **B** Examples of macroscopic I_j obtained with the standard pulse protocol. Voltage steps were applied to cell 1 and I_j recorded from cell 2. **C** Dependence of $g_{j,ss}$ on V_j. The mixed-Cx43 pairs exhibit homogenous behaviour for hyperpolarization, but not for depolarization of cell 1. Each *symbol* represents a single cell pair. The *curve* for the data at $V_j>0$ mV corresponds to the best fit of data to Eq. 2 (for details, see text)

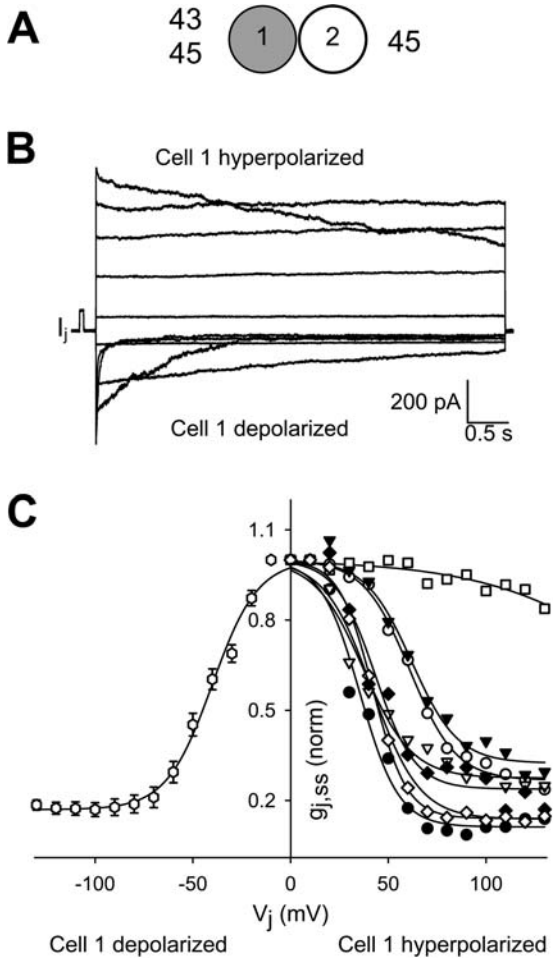

Fig. 6A–C Dependence of the steady-state gap junction conductance on junctional potential of mixed-Cx45 cell pairs consisting of a co-transfected cell (Cx43/45) and a singly transfected cell (Cx45). **A** Cell-pair configuration. **B** Examples of macroscopic I_j for the standard V_j pulse protocol. Voltage steps were applied to the cell 1 and I_j recorded from cell 2. **C** Dependence of $g_{j,ss}$ on V_j. The mixed-Cx45 pairs exhibited homogenous behaviour for depolarization of cell 1, but not for hyperpolarization. Each *symbol* represents a single cell pair. The *curve* for the data at V_j<0 mV shows the best fit of data to Eq 2 (for details, see text)

$g_{j,ss}$=f(V_j) for seven selected Cx43/45-Cx45 cell pairs. The plots followed a distinct pattern of voltage gating. When cell 1 was depolarized, the function was similar in each preparation. Pooling and averaging the data yielded a unique curve with the following Boltzmann parameters (negative V_j): $V_{j,0}$=−40.1±1.2 mV, $g_{j,min}$=0.17±0.014, z=−2.2±0.18. When cell 1 was hyperpolarized (the homomeric Cx45 connexons in cell 2 were positive), the function $g_{j,ss}$=f(V_j) was different in each cell pair. Likewise, the V_j polarity that generated the unique function $g_{j,ss}$=f(V_j) gave rise to similar $g_{j,inst}$ data in each cell pair (data omitted for clarity). The analysis of the averaged data yielded the following values (negative V_j): G_j=1.99±0.009, V_H=−124.5±1.8 mV. Starting from 1.0 at V_j=0 mV, $g_{j,inst}$ decreased to 0.79 at V_j=−100 mV. Similarly, the V_j polarity that yielded heterogeneous functions $g_{j,ss}$=f(V_j) gave rise to different $g_{j,inst}$ data in each preparation (data omitted for clarity). The cell pairs included in the analysis had an average $g_{j,inst}$ of 4.2±0.6 nS at V_j=0 mV (n=27). Preparations with $g_{j,inst}$>16 nS were discarded.

Voltage dependence of g_j in Cx43/45-Cx43/45 cell pairs

Another series of experiments was carried out on pairs in which each cell co-expressed Cx43 and Cx45 (Fig. 7A). Each preparation studied showed a different pattern of current signals. The panels in Fig. 7B show families of current records obtained from four selected preparations. In each case, the sequence of voltage steps was identical, i.e. V_j=±10, ±40, ±70, ±100 and ±130 mV. The panel on the upper left shows I_j signals that were nearly symmetrical with regard to V_j polarity. They resemble those of homomeric Cx45-Cx45 cell pairs (Fig. 3B). The panel on the upper right shows currents which exhibited some degree of asymmetry. Moreover, the traces at V_j=±100 mV exhibited an unusual time-dependent decay. The panel on the lower left shows strongly asymmetrical currents. In this case, I_j decreased prominently at negative V_j and marginally at positive V_j. The panel on the lower right shows a case with nearly symmetrical currents. However, inactivation began at large V_j only. Moreover, some currents showed a rapid inactivation followed by a slow activation.

Figure 7C shows plots of the function $g_{j,ss}$=f(V_j) gained from the analysis of selected experiments (symbols represent different preparations). The smooth curves correspond to the best fit of data to Eq. 2. The left-hand panel shows examples with a nearly symmetrical behaviour. It indicates the range of V_j sensitivities observed. For the four cases documented, the data analysis yielded the following Boltzmann parameters (negative/positive V_j for open triangles, circles, squares and diamonds): $V_{j,0}$= −31.2/29.6, −55.1/52.6, −60.5/67.1 and −35.4/36.1 mV; $g_{j,min}$=0.08/0.07, 0.21/0.20, 0.29/0.29, and 0.11/0.11; z= −2.0/1.8, −3.6/2.8, −1.5/1.3 and −5.2/2.8 respectively. The right-hand panel shows selected examples with an asymmetrical behaviour. For the three cases illustrated, the Boltzmann parameters were as follows (for solid triangles, circles and squares): $V_{j,0}$=−58.6/73.5, −28.6/93.4, and −53.3/60.9 mV; $g_{j,min}$=0.31/0.74, 0.13/0.35 and 0.16/0.27; z=−2.8/1.5, −4.1/1.5 and −2.0/4.1 respectively. The function $g_{j,inst}$=f(V_j) varied considerably among the different preparations. Hence, these data were omitted in Fig. 7C.

Compiled data on voltage gating

We have examined 93 preparations in which cells co-expressed Cx43 and Cx45 (see above). Each cell pair behaved differently, thus yielding a unique set of Boltzmann parameters. In 38% of the cases, the relationship $g_{j,ss}$=f(V_j) was quasi-symmetrical (n=35), in 62% of the cases asymmetrical (n=58). Figure 8 illustrates the results of selected experiments in graphical form empha-

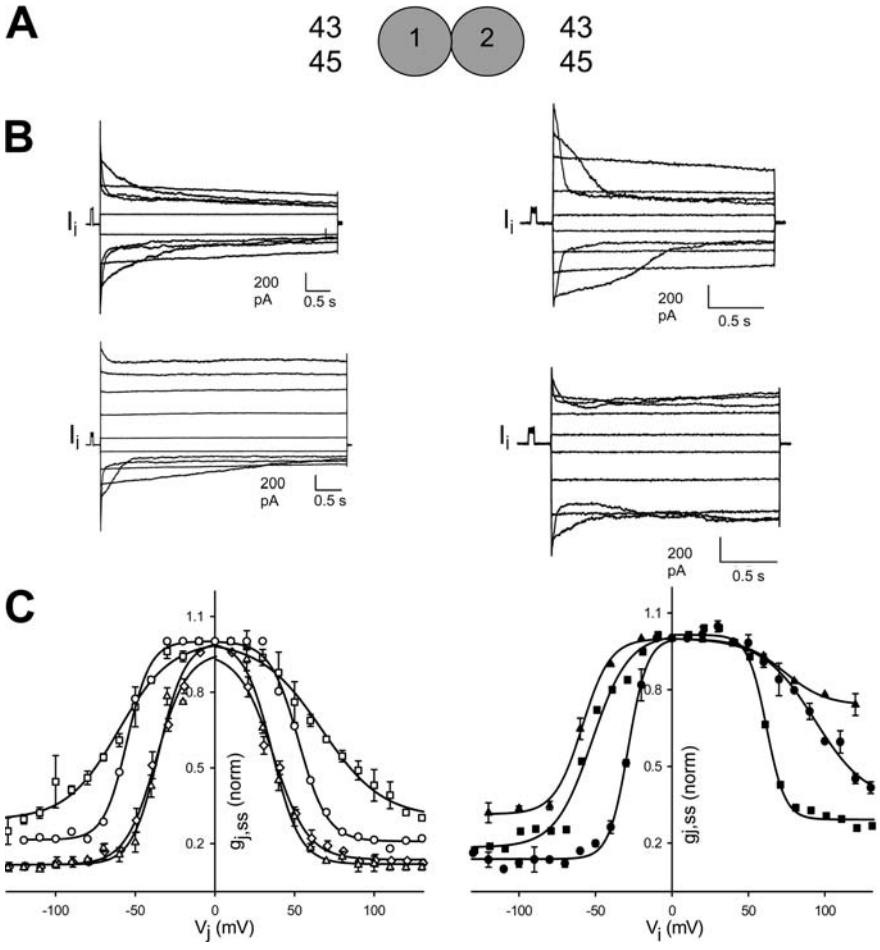

Fig. 7A–C Dependence of the steady-state gap junction conductance on junctional potential of cell pairs in which each cell co-expresses Cx43 and Cx45. **A** Cell-pair configuration. **B** Examples of current records gained with the standard pulse protocol. Each preparation yielded a different set of I_j records: quasi-symmetrical or non-symmetrical (compare *panels* on the *left-hand side*), high or low voltage sensitivity (compare *panels* in the *upper row*), monophasic or biphasic time-course (compare *upper left-hand panel* with *lower right-hand panel*). **C** Dependence of $g_{j,ss}$ on V_j for selected cases giving rise to quasi-symmetrical (*left-hand side*) or asymmetrical relationships (*right-hand side*). Each *symbol* represents a single cell pair. The *curves* correspond to the best fit of data to Eq. 2 (for details, see text)

sizing the range of data. Figure 8A–C shows the parameters $V_{j,0}$, $g_{j,min}$ and z, respectively, represented by the end-points of vertical bars (upper end/lower end: data for positive/negative V_j). The left-hand panels show cases with quasi-symmetrical behaviour, the middle panels cases with asymmetrical behaviour. For clarity, the number of experiments depicted was reduced to 17 and 32, respectively. Missing data indicate the limits of the analysis procedure. The preparations analysed had an average $g_{j,inst}$ of 5.1±0.4 nS at V_j=0 mV (n=93; see also Table 1). Cell pairs with $g_{j,inst}$>13 nS were discarded. The right-hand panels summarize the data of the other types of cell pairs examined, i.e. the reference cell pairs Cx43-Cx43 and Cx45-Cx45, the Cx43-Cx45 cell pairs and the Cx43/45-Cx43 and Cx43/45-Cx45 cell pairs (see also Table 1). In the latter two cases, the data presented refer to the V_j polarity giving rise to homogeneous $g_{j,ss}$ responses.

For Cx43/Cx45-Cx43/Cx45 cell pairs (Fig. 8, left-hand panels and middle panels), $|V_{j,0}|$ was 28–114 mV, $g_{j,min}$ 0.10–0.75 and $|z|$ 0.8–6.4 (see also Table 1). These values are well beyond those of homomeric-homotypic channels (Fig. 8, right-hand panels). Conceivably, the range of data reflects the variable level of connexin expression giving

Table 1 Boltzmann parameters determined from different types of cell-pairs. Data are given as mean values (exception: Cx43/45-Cx43/45 cell pairs: range of absolute values) ($V_{j,0}$: V_j at which $g_{j,ss}$/$g_{j,inst}$ is the half-maximally inactivated; $g_{j,min}$: minimal conductance at large V_j; z: number of unitary positive charges q movin through the electric field applied; ND: mean value not determined due broad range of data

Cell-pair configuration	$V_{j,0}$ (mV)	$g_{j,min}$	z
Cx43-Cx43	−60.8/62.9	0.26/0.25	−3.4/2.9
Cx45-Cx45	−38.9/38.5	0.17/0.16	−2.5/2.7
Cx43-Cx45	−11.7/134.4	0.05/ND	−2.1/0.6
Cx43/45-Cx43	ND/49.7	ND/0.16	ND/1.5
Cx43/45-Cx45	−40.1/ND	0.17/ND	−2.2/ND
Cx43/45-Cx43/45	28–114	0.10–0.75	0.8–6.4

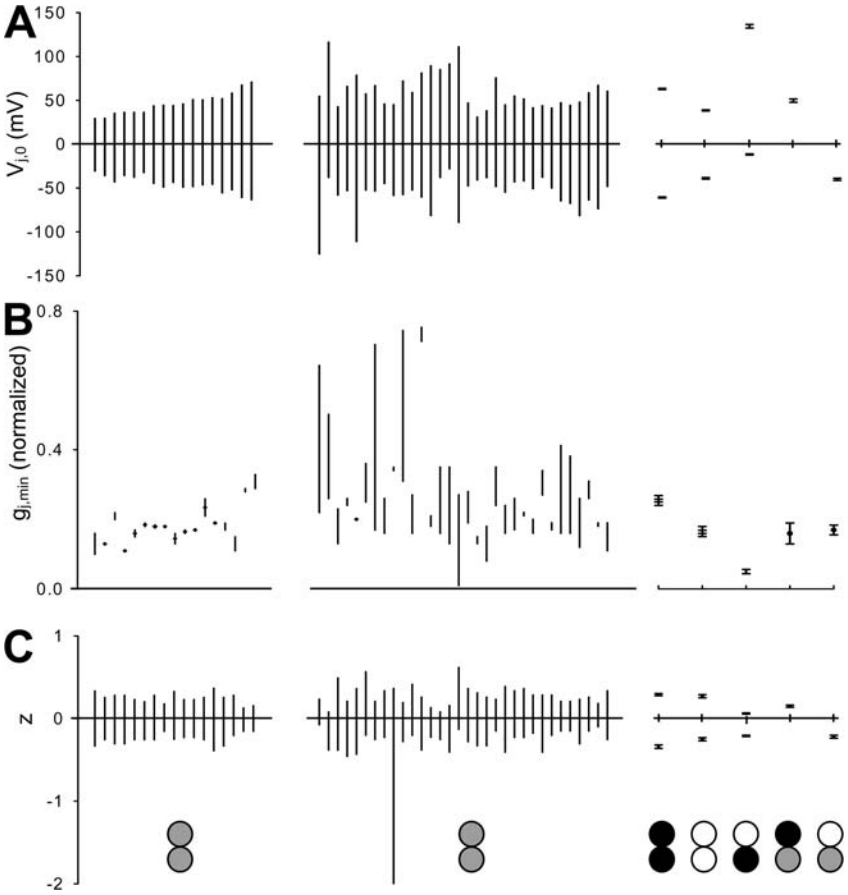

Fig. 8A–C Compiled data on voltage gating of cell pairs, both cells of which co-express Cx43 and Cx45. The *ends* of the *vertical bars* represent the values of $V_{j,0}$ (V_j at which $g_{j,ss}/g_{j,inst}$ is half-maximally inactivated, **A**), $g_{j,min}$ (minimum g_j at large V_j, **B**) and z (number of unitary positive charges moving through applied electric field, **C**). In the case of $V_{j,0}$ and z, the upper/lower end of each bar corresponds to the respective value at positive/negative V_j, i.e. y=0 separates the data for different V_j polarity. *Left-hand panels*: data for selected cell pairs with quasi-symmetrical V_j sensitivity (n=17 out of 35); *middle panels* (n=32 out of 56): data for selected cell pairs with asymmetrical $V_{j,0}$ sensitivity. The experiments were selected to document the range of data. *Right-hand panels*: data from the other cell pair configurations, i.e. Cx43-Cx43, Cx45-Cx45, Cx43-Cx45, Cx43/45-Cx43 and Cx43/45-Cx45 (from *left* to *right*; for details, see text). *Insets* in **C**: cell-pair configuration (cell1/cell2: *lower/upper circle*; *black* Cx43; *white* Cx45; *grey* Cx43/45)

rise to the formation of a broad spectrum of different types of gap junction channels.

Kinetics of I_j inactivation

The current signals were also used to analyse the kinetics of I_j inactivation. For Cx43-Cx43 and Cx45-Cx45 cell pairs, I_j decayed with time as a single exponential ($|V_j|$<90 mV) or the sum of two exponentials ($|V_j|\geq$90 mV; data not shown) giving rise to the time constants τ_{i1} or τ_{i1} and τ_{i2}, respectively. For Cx43-Cx45 cell pairs, the inactivation of I_j showed a similar pattern with one or two time constants when the Cx43 connexon was depolarized. Figure 9A shows a representative example with τ_{i1} and τ_{i2} of 24.8 and 355 ms, respectively, at V_j=100 mV. Due to the complex shape of the I_j signals, no time constants could be determined when the Cx45 connexon was depolarized (Fig. 4A). For Cx43/Cx45-Cx43 and Cx43/45-Cx45 cell pairs, I_j also showed one or two time constants for the V_j polarity which yielded uniform I_j responses, i.e. when the homomeric Cx43 connexon was depolarized or the homomeric Cx45 connexon was hyperpolarized, respectively (data not shown, but see Figs. 5A and 6A). For the opposite V_j polarity, no meaningful analysis could be made because of the variable behaviour of I_j.

Figure 9B shows plots of the function τ_{i1}=f(V_j) for the different kinds of cell pairs. Where appropriate, the values for negative and positive V_j were pooled. The data obtained were best approximated by single exponentials. The curve-fitting procedure yielded two parameters that characterize the inactivation, the intercept at V_j=0, $\tau_{i,0}$, and the decay constant V_τ. The Cx43-Cx43 (solid circles) and Cx45-Cx45 (open circle) cell pairs yielded the following values: $\tau_{i,0}$=72.2 s, V_τ=14.8 mV; and $\tau_{i,0}$=132.3 s, V_τ=13.5 mV, respectively. This indicates that the Cx43-Cx43 channels inactivated more rapidly than the Cx45-Cx45 channels. The Cx43-Cx45 cell pairs yielded the following values when the Cx45 connexon was hyperpolarized (solid triangles): $\tau_{i,0}$=109.9 s; V_τ=11.8 mV. Hence, the inactivation of I_j was faster than that of the Cx43-Cx43 or Cx45-Cx45 channels. The Cx43/45-Cx43 cell pairs, in the case of depolarizing the Cx43 connexons, gave the following values (open inverse triangles): $\tau_{i,0}$=18.8 s, V_τ=18.9 mV; likewise, the Cx43/45-Cx45 cell pairs, in the case of hyperpolarizing the Cx45 connexons, led to the following values (solid squares): $\tau_{i,0}$=136.9 s, V_τ=12.5 mV. Thus, the inactivation of I_j was faster than that of the respective Cx43-Cx43 or Cx45-Cx45 channels.

Computations of the function $g_{j,ss}$=f(V_j)

Based on the data gained from the Cx43-Cx43, Cx45-Cx45 and Cx43-Cx45 cell pairs, an attempt was made to predict the properties of mixed gap junctions consisting of

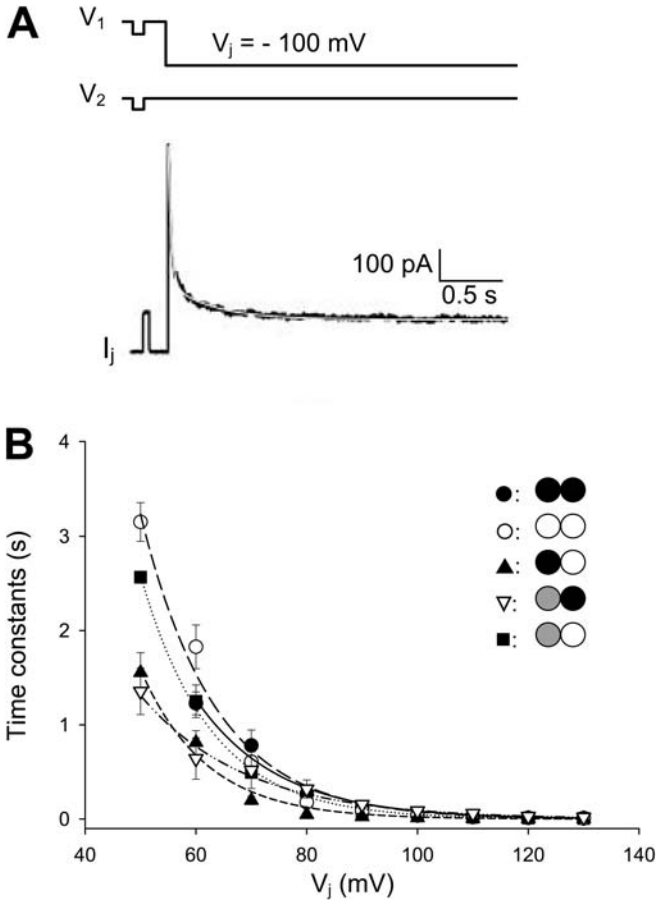

Fig. 9A, B Kinetics of I_j inactivation. **A** Current signal I_j recorded from a mixed-Cx43 cell pair at V_j=100 mV (V_1=−100 mV, V_2=0 mV). I_j decayed with time following the sum of two exponentials giving rise to two time constants (τ_{i1}=24.8 ms; τ_{i2}=355 ms). **B** τ_{i1} as a function of V_j for I_j obtained from different types of cell pairs: homotypic Cx43-Cx43 (●; *n*=9); homotypic Cx45-Cx45 (○; *n*=12); heterotypic Cx43-45 in the case of depolarization of the Cx43 cell (▲; *n*=9); mixed-Cx43 (▽; *n*=22) and mixed-Cx45 (■; *n*=26) for their homogenous behaviour. The *curves* correspond to the best fit of data to a single exponential. *Inset*: cell-pair configuration (cell1/cell2: *left hand/right hand circle*; *black* Cx43; *white* Cx45; *grey* Cx43/45)

different fractions of homomeric-homotypic and homomeric-heterotypic channels, but no heteromeric-homotypic or heteromeric-heterotypic channels (Fig. 1). It was assumed that the resulting channels do not interact functionally. For this purpose, the functions $g_{j,ss}$=f(V_j) obtained from the Cx43-Cx43, Cx45-Cx45 and Cx43-Cx45 cell pairs were used as reference. The behaviour of mixed gap junctions was then determined by addition of the respective functions at appropriate weight and orientation (Eq. 3). The insets in Fig. 10 show the connexon combinations considered (black box: Cx43; white box: Cx45; left-hand box: cell 1, right-hand box: cell 2). The numbers 1 and 2 indicate the respective channel configuration.

Figure 10A and B illustrates the case when Cx43/Cx45 cells were paired. The family of curves in Fig. 10A document the situation in which only homotypic combinations were allowed. Curves (a) and (e) correspond to the experimentally determined properties of 100% Cx43-Cx43 and 100% Cx45-Cx45 channels, respectively (solid curves with data points). The computed curves (dashed curves) in between represent the functions with 75% Cx43-Cx43 and 25% Cx45-Cx45 channels (b), 50% Cx43-Cx43 and 50% Cx45-Cx45 channels (c) and 25% Cx43-Cx43 and 75% Cx45-C45 channels (d). Each curve was symmetrical and invariant to channel orientation. The curves in Fig. 10B document the situation in which only heterotypic combinations were allowed. Curves (a) and (e) correspond to the experimentally determined properties of 100% Cx43-Cx45 channels inserted at inverse orientation. The prominent asymmetry of these curves gradually disappeared when the differently oriented channels were mixed (curve b: 75% 1 and 25% 2; curve d: 25% 1 and 75% 2). It was gone completely in the presence of 50% at each orientation (c).

Figure 10C and D illustrates the case when Cx43/45 cells were paired with Cx43 or Cx45 cells. In both cases, homotypic and heterotypic combinations were allowed. In Fig. 10C, curves (a) and (e) depict the experimentally determined properties of 100% Cx43-Cx43 and 100% Cx45-Cx43 channels exhibiting a symmetry and asymmetry, respectively. Curves b–d document the transitions between the two reference functions. In Fig. 10D, curves (a) and (e) represent the experimentally determined behaviour of 100% Cx45-Cx45 and 100% Cx43-Cx45 channels showing symmetry and asymmetry, respectively. The curves b–d represent the functions when the two kinds of channels are mixed stepwise. Note that the rectification of the functions (d) in Fig. 10D and E is opposite.

Discussion

Cx43-Cx43 and Cx45-Cx45 cell pairs

The homotypic Cx43-Cx43 and Cx45-Cx45 cell pairs yielded homogeneous results (Figs. 2C and 3C). Hence, both delivered a unique set of Boltzmann parameters (Table 1). The values of $V_{j,0}$ and $g_{j,min}$ suggest that Cx43-Cx43 channels are less voltage sensitive and have a larger minimum conductance than Cx45-Cx45 channels. This is consistent with previous studies on injected *Xenopus* oocytes [3], transfected human HeLa cells [2, 12] and mammalian cell lines [22]. The observation that $g_{j,min}\neq 0$ indicates that the channels remain in a residual state at large V_j [12, 28].

Both types of channels, moreover, inactivated voltage-dependently and following a single or double exponential time course, thus giving rise to a single (τ_{i1}), or two time constants (τ_{i1} and τ_{i2}) respectively (Fig. 9B). τ_{i1} decreased with increasing V_j, i.e. the larger the voltage, the faster the inactivation. Data comparison indicates that Cx43-Cx43 channels inactivated more rapidly than Cx45-Cx45 channels for voltages allowing a meaningful comparison, i.e. $V_j \geq |50|$ mV (the lower limit for obtaining a reliable τ_{i1}) and $V_j \leq |90|$ mV (the upper limit for establishing a significant difference in τ_{i1}). These findings are consistent

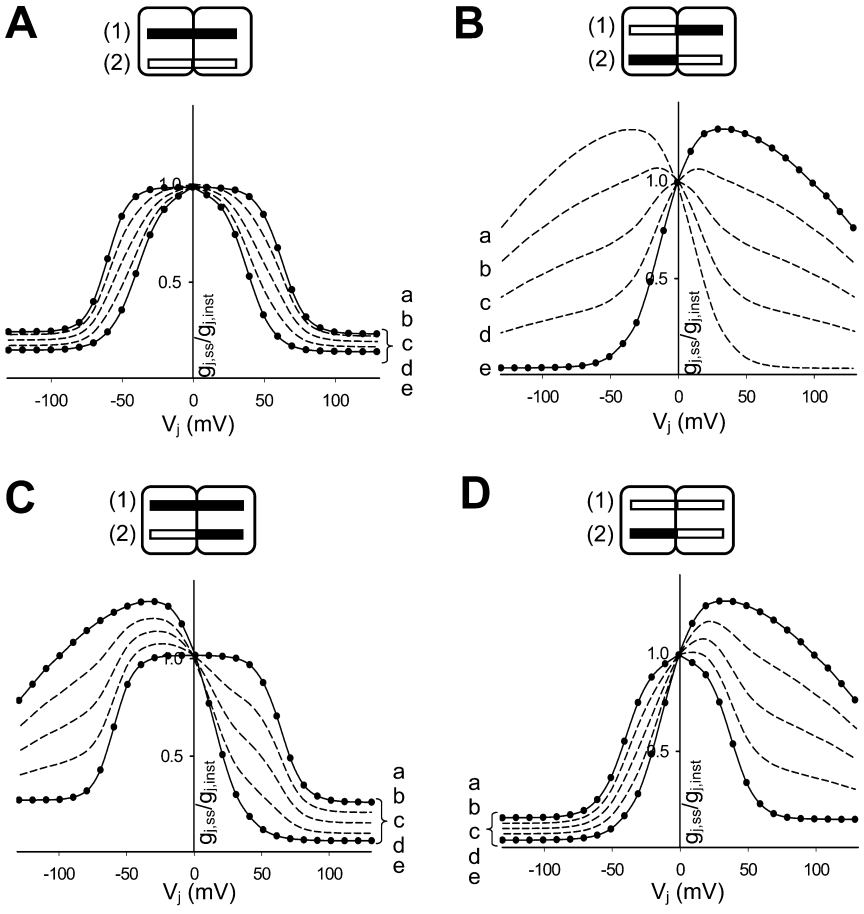

Fig. 10A–D Computed functions of $g_{j,ss}=f(V_j)$, assuming gap junction channels to consist of homomeric Cx43 and Cx45 connexons. The computations are based on the experimental data of Cx43-Cx43, Cx45-Cx45 and Cx43-Cx45 cell pairs. *Insets*: scheme of connexon combinations; *black box* Cx43; *white box* Cx45; *left-hand side* cell 1, *right-hand side* cell 2; *numbers 1* and *2* types of channels. *Solid curves* experimental data; *dashed curves* computed data. Curves *a–e* illustrate the behaviour for different mixtures of gap junction channels (channel type 1/channel type 2): 100/0%, 75/25%, 50/50%, 25/75% and 0/100%. **A** Cx43/Cx45-Cx43/45 cell pair, allowing homotypic channels only. **B** Cx43/45-Cx43/45 cell pair, allowing heterotypic channels only. **C** Cx43/45-Cx43 cell pair, allowing homotypic and heterotypic channels. **D** Cx43/45-Cx45 cell pair, allowing homotypic and heterotypic channels

with previous reports on Cx43-Cx43 and Cx45-Cx45 channels [2, 3, 12, 22].

Cx43-Cx45 cell pairs

For heterotypic Cx43-Cx45 cell pairs, the functions $g_{j,inst}=f(V_j)$ and $g_{j,ss}=f(V_j)$ exhibited moderate and pronounced rectification, facilitating current flow from cell 2 to cell 1 and impeding it from cell 1 to cell 2, respectively (Fig. 4C). This is consistent with previous studies [12, 22, 25, 31]. When depolarizing pulses were applied to the Cx43 connexons (negative V_j), the curvature of the functions resembled those of homotypic channels. However, close inspection indicates that both dependence of $g_{j,inst}$ and $g_{j,ss}$ on V_j as well as the kinetics of I_j differed from the corresponding properties of Cx43-Cx43 or Cx45-Cx45 channels (compare Figs. 2C and 3C with Fig. 4C). The parameters $V_{j,0}$ and $g_{j,min}$ obtained for the Cx43-Cx45 channels were smaller than those of either type of homotypic channel, indicating that both connexons responded concomitantly (Table 1). These findings are compatible with the assumption that Cx43 and Cx45 connexons gate with positive and negative voltage, respectively. Moreover, when depolarizing pulses were applied to the Cx43 connexons (negative V_j), the Cx43-Cx45 channels inactivated more rapidly than either type of homotypic channel (Fig. 9B). This is also consistent with concurrent gating of the Cx43 and Cx45 connexons. Hyperpolarization of cell 1 (positive V_j) elicited a transient increase in I_j followed by a moderate decrease. Conceivably, the initial increase represents the opening of channels that were in the residual state at V_j=0 mV. Hence, negative V_j consumes a significant fraction of gating capacity leaving but little at positive V_j. The decrease of $g_{j,ss}$ at more positive V_j may be due the voltage dependence of the channel main state and a gating mechanism similar to that observed in solitary connexons [26, 30].

While this interpretation is consistent with current knowledge on gap junction channels, it conflicts with other connexon data. Recently, it has been reported that Cx45 and Cx43 hemichannels gate with negative voltage [1, 7, 27]. To rescue the foregoing interpretation, it would have to be assumed that hemichannel docking inverts the gating polarity of one of the connexins, probably the Cx43. Previously, it has been proposed that the function $g_{j,ss}=f(V_j)$ of Cx43-Cx45 cell pairs results from negative gating of both connexons [12, 22, 25, 31]. Hence, depolarization of cell 1 (negative V_j) would involve the operation of Cx45 connexons and hyperpolarization (positive V_j) the operation of Cx43 connexons. While this interpretation is consistent with the current knowledge on hemichannels (see above), it also conflicts with gap junction channel data. To save this concept, extra arguments are needed. For example, to account for the function $g_{j,ss}=f(V_j)$, docking would have to shift the

voltage sensitivity of the Cx43 connexons by more than 100 mV (compare [7, 12]) or there would be no voltage window for channels in the main state, i.e. the channels would always be in a conformation with one or both connexins in the residual state. The same would be true for the function $g_{j,ss}=f(V_j)$ of Cx43-Cx43 cell pairs. Moreover, $g_{j,min}$ at large negative V_j would have to increase above the level inherent to Cx45-Cx45 channels. Yet, it decreased (compare Figs. 3C and 4C) or even disappeared [12]. In brief, both interpretations presented require assumptions beyond the currently accepted properties of gap junction channels or hemichannels. Nevertheless, simply to discuss the subsequent data (see below), we will restrict ourselves to one of the concepts, namely the first, since we favour it at this stage. Prominent asymmetrical functions $g_{j,inst}=f(V_j)$ and $g_{j,ss}=f(V_j)$ have also been observed in the case of other heterotypic Cx combinations relevant for cardiac tissue, i.e. Cx40-Cx43 [16, 31] and Cx40-Cx45 [31].

Cx43/45-Cx43 and Cx43/45-Cx45 cell pairs

The studies with the Cx43/45-Cx43 and Cx43/45-Cx45 cell pairs revealed functions $g_{j,ss}=f(V_j)$ that varied between preparations. Typically, one voltage polarity yielded quasi-homogeneous data, the other heterogeneous data. Hence, the degree of rectification varied from cell pair to cell pair. Based on the framework used to interpret the Cx43-Cx45 data (see Cx43-Cx45 cell pairs), the properties of the mixed cell pairs can be explained as follows.

For Cx43/45-Cx43 cell pairs, hyperpolarization of cell 1 (positive V_j) led to quasi-homogeneous behaviour (Fig. 5C). Assuming that Cx43 and Cx45 gate with positive and negative voltage, respectively, this behaviour reflects the gating of Cx43-Cx43 (involving Cx43 of connexon 2) and Cx43/45-Cx43 channels (involving Cx43 of connexon 2 and Cx45 of connexon 1). This is consistent with the finding that the Boltzmann parameters of the Cx43/45-Cx43 cell pairs were intermediate between those of the Cx43-Cx43 and Cx43-Cx45 cell pairs (Table 1). Hence, the contour of $g_{j,ss}=f(V_j)$ may be expected to range from that of Cx43-Cx43 (Fig. 2C) to that of Cx43-Cx45 channels (Fig. 4C, negative V_j), depending on the ratio of Cx expression in cell 1 and the formation of heterotypic channels. However, such extreme cases were not observed, i.e. the experimental data varied rather little and hence were averaged. This led to the S-shaped curve with standard errors slightly larger than those e.g. of Cx43-Cx43 cell pairs (compare Figs. 2C and 5C). Furthermore, I_j inactivated more rapidly in Cx43/45-Cx43 than in Cx43-Cx43 cell pairs (Fig. 9B). This may indicate a contribution of channels containing Cx45.

In contrast, depolarization of cell 1 (negative V_j) gave rise to prominent heterogeneous behaviour (Fig. 5C). This reflects the gating of Cx43-Cx43 channels (involving Cx43 of connexon 1) and the V_j dependence of the channel main state superimposed on an extra gating mechanism of channels containing Cx43 and Cx45 (see Cx43-Cx45 cell pairs). Thus, the shape of $g_{j,ss}=f(V_j)$ may be expected to range from that of Cx43-Cx43 (Fig. 2C) to that of Cx43-Cx45 channels (Fig. 4C, positive V_j), with intermediates depending on the expression level of Cx43 and Cx45 in cell 1 and the formation of heterotypic channels. The data in Fig. 5 are consistent with this interpretation.

For Cx43/45-Cx45 cell pairs, the function $g_{j,ss}=f(V_j)$ was inverted. Depolarization of cell 1 (negative V_j) yielded nearly homogenous behaviour (Fig. 6C), reflecting the gating of Cx45-Cx45 (involving Cx45 of connexon 2) and Cx43/45-Cx45 channels (involving Cx43 of connexon 1 and Cx45 of connexon 2). This is consistent with the finding that the Cx43/45-Cx43 cell pairs yielded Boltzmann parameters between those of the Cx45-Cx45 and Cx43-Cx45 cell pairs (Table 1). Thus, the contour of $g_{j,ss}=f(V_j)$ may be expected to range from that of Cx45-Cx45 (Fig. 3C) to that of Cx43-Cx45 channels (Fig. 4C, negative V_j), depending on the ratio of Cx expression in cell 1 and the formation of heterotypic channels. Moreover, I_j inactivated more rapidly in Cx43/45-Cx45 cell pairs than in Cx45-Cx45 cell pairs (Fig. 9B). This indicates a contribution of channels containing Cx43. In contrast, hyperpolarization of cell 1 (positive V_j) gave rise to prominent, heterogeneous behaviour, reflecting the gating of Cx45-Cx45 channels (involving Cx45 of connexon 1) and the V_j dependence of the channel main state superimposed on an extra gating mechanism of channels containing Cx43 and Cx45 (see Cx43-Cx45 cell pairs). Therefore, the shape of $g_{j,ss}=f(V_j)$ may be expected to range from that of Cx45-Cx45 (Fig. 3C) and that of Cx43-Cx45 channels (Fig. 4C, positive V_j), with intermediate cases depending on the expression level of Cx43 and Cx45 in cell 1 and the formation of heterotypic channels. The data in Fig. 6 are compatible with these explanations.

Cx43/45-Cx43/45 cell pairs

The experiments with Cx43/45-Cx43/45 cell pairs gave a broad spectrum of I_j responses (Fig. 7B). Besides conventional monotonic decays, we observed non-monotonic decays and transient decreases followed by subsequent increases. The resulting functions $g_{j,ss}=f(V_j)$ differed from preparation to preparation. Depolarization of cell 1 (negative V_j) yielded heterogeneous behaviour (Fig. 7C) reflecting the gating of channels containing Cx43 in connexon 1 and/or Cx45 in connexon 2. Possible candidates are the Cx43-Cx43, Cx43-Cx45, Cx43-Cx45/43, Cx45-Cx45, Cx43/45-Cx45 and Cx43/45-Cx43/45 channels. Hence, the contour of $g_{j,ss}=f(V_j)$ can be expected to range from that of Cx43-Cx43 (Fig. 2C) to that of Cx45-Cx45 (Fig. 3C) and Cx43-Cx45 channels (Fig. 4C), depending on the ratio of Cx expression in cell 1 and cell 2. Likewise, hyperpolarization of cell 1 (positive V_j) yielded heterogeneous behaviour (Fig. 7C) reflecting the gating of channels containing Cx45 in connexon 1 and/or Cx43 in connexon 2. Again, six different classes of channels may have been involved.

The functions $g_{j,ss}=f(V_j)$ observed can be divided into two groups, those with quasi-symmetrical and those with

asymmetrical behaviour (Figs. 7C and 8). The first group includes profiles similar to those of Cx43-Cx43 and Cx45-Cx45 channels. The cells of these preparations may have been nearly identical with regard to Cx expression, thus leading to a symmetrical arrangement of different types of channels. The second group includes profiles resembling those of Cx43/45-Cx43 and Cx43/45-Cx45 channels. The cells of these preparations may have expressed Cx43 and Cx45 at different levels, thus resulting in asymmetrical arrangements of different types of channels. Because of the broad spectrum of voltage profiles encountered, the data gained from Cx43/45-Cx43/45 cell pairs were not averaged. Instead, the Boltzmann parameters of selected experiments were presented to document the range of data (Fig. 8, left-hand panels and middle panels; see also Table 1). The variability suggests that each cell exhibited a different pattern of Cx expression, presumably correlated with the cell cycle.

Identification of types of channel in complex gap junctions

The data gained from Cx43-Cx43, Cx45-Cx45 and Cx43-Cx45 cell pairs (Figs. 2C, 3C and 4C) have been used to predict the properties of mixed gap junctions consisting of homomeric connexons (Fig. 10). For Cx43/45-Cx43 cell pairs, the experimentally determined functions $g_{j,ss}=f(V_j)$ are not easy to reconcile with the predicted ones (compare Figs. 5C and 10C), even when the extreme cases are ignored, i.e. traces (a) and (e) in Fig. 10C (for an argument, see Cx43/45-Cx43 and Cx43/45-Cx45 cell pairs). While this narrows down the profiles at positive V_j, it does not explain adequately the range and shape of the profiles observed at negative V_j. This discrepancy may indicate the presence of channels containing heteromeric connexons in cell 1. For Cx43/45-Cx45 cell pairs, comparison leads to a similar conclusion (compare Figs. 6C and 10D). Ignoring the extreme cases (a) and (e) in Fig. 10D narrows down sufficiently the predicted profiles at negative V_j but does not explain the range and shape of the experimentally determined profiles at positive V_j. Again, this may indicate the presence of heteromeric connexons in cell 1 and hence corresponding gap junction channels.

For Cx43/45-Cx43/45 cell pairs, a comparison between experimental data and computed predictions is even more difficult due to the larger number of possible channel configurations (compare Figs. 7C and 8 with Fig. 10). The preponderance of asymmetrical (62%) over symmetrical cases (38%) suggests a certain variation of Cx expression among the cells (Fig. 8, left-hand and middle panels). Hence, in Fig. 10A–D curves b–d would be more appropriate than the curves (a) and (e). In the symmetrical cases, one might expect a contribution of the predicted profiles in Figs. 10A and B (preferentially the curves (c) or close neighbours thereof) plus those in Figs. 10C and D (preferentially the curves (c) or close neighbours thereof). Such profiles predict biphasic decays of $g_{j,ss}$, behaviour not observed experimentally (Fig. 7C, left-hand panel). In the asymmetrical cases, one might expect primarily a contribution of the predicted profiles in Figs. 10C and D (preferentially the curves (c) or close neighbours thereof). This also would give rise to biphasic decays of $g_{j,ss}$, a property not seen in the experiments (Fig. 7C, right-hand panel). Hence, in both groups of cell pairs, the discrepancy between experimental and predicted data may be due to the presence of channels containing heteromeric connexons.

The diversity of voltage profiles observed in the present study is consistent with that of previous studies involving Cx40, Cx43 and Cx45 [9, 16, 23, 32] and Cx37 and Cx43 [4]. From these studies it was inferred that heteromeric channels exist or may exist.

Physiological significance

Gap junction channels play a crucial role for the propagation of the cardiac impulse [20]. The current concept assumes a positive correlation between the number of gap junction channels and the conduction velocity. However, this scheme is incomplete. The conduction velocity depends not only on the number of channels, but also on the type of channels and their orientation in a tissue. Depending on the type of channels and their orientation, the impulse propagation can be facilitated (signal transfer: C45→Cx43, Cx43/45→Cx43 or Cx45→Cx43/45) or impaired (signal transfer: Cx43→Cx45) due to the rectification of $g_{j,inst}$ and $g_{j,ss}$. Hence, of particular interest are tissue areas where cells expressing Cx43 and/or Cx45 make contact with each other. Prominent examples are auricular muscle (Cx43-Cx45, Cx43/45-Cx43/45) and Purkinje fibres (Cx43-Cx45, Cx43/45-Cx43/45) or the transitional zone at the junctions SA node-auricular muscle (Cx45-Cx43, Cx45-Cx43/45), auricular muscle-AV node (Cx43-Cx45, Cx43/45-Cx45), bundle branches-Purkinje fibres (Cx45-Cx43, Cx45-Cx43/45) and Purkinje fibres-ventricular muscle (Cx45-Cx43, Cx43/45-Cx43) [8, 10, 17] (for review, see [34]).

Acknowledgements We thank the laboratory of K. Willecke, Institut für Genetik, Bonn, Germany, for providing some transfected cells. We are grateful to D. Lüthi for expert technical assistance. This work was supported by grants of the Bundesamt für Bildung und Wissenschaft (code 99.0368-1; code EU grant: QLG1-GT-199-00516) and the Swiss National Science Foundation (31-55297.98 and 31-67230.01).

References

1. Bader P, Weingart R (2003) Conductive and kinetic properties of connexin45 hemichannels (abstract). Pflugers Arch 445:R69
2. Banach K, Weingart R (2000) Voltage gating of Cx43 gap junction channels involves fast and slow current transitions. Pflugers Arch 439:248–250
3. Barrio LC, Capel J, Jarillo JA, Castro C, Revilla A (1997) Species-specific voltage-gating properties of connexin-45 junctions expressed in Xenopus oocytes. Biophys J 73:757–769

4. Brink PR, Cronin K, Banach K, Peterson E, Westphale EM, Seul KH, Ramanan SV, Beyer EC (1997) Evidence for heteromeric gap junction channels formed from rat connexin43 and human connexin37. Am J Physiol 273:C1386–C1396
5. Bruzzone R, White WT, Paul DL (1996) Connection with connexins: the molecular basis of direct intercellular signaling. Eur J Biochem 138:1–27
6. Chen-Izu Y, Moreno AP, Spangler RA (2001) Opposing gates model for voltage gating of gap junction channels. Am J Physiol 281:C1604–C1613
7. Contreras JE, Saez JC, Bukauskas FF, Bennett MVL (2003) Gating and regulation of connexin 43 (Cx43) hemichannels. Proc Natl Acad Sci USA 100:11388–11393
8. Coppen SR, Kodama I, Boyett MR, Dobrzynski H, Takagishi Y, Honjo H, Yeh HI, Severs NJ (1999) Connexin45, a major connexin of the rabbit sinoatrial node, is co-expressed with connexin43 in a restricted zone at the nodal-crista terminalis border. J Histochem Cytochem 47:907–918
9. Cottrell GT, Wu Y, Burt JM (2002) Cx40 and Cx43 expression ratio influences heteromeric/heterotypic gap junction channel properties. Am J Physiol 282:C1469–C1482
10. Davis LM, Rodefeld ME, Green K, Beyer EC, Saffitz JE (1995) Gap junction protein phenotypes of the human heart and conduction system. J Cardiovasc Electrophysiol 6:813–822
11. Desplantez T, Weingart R (2003) Connexins Cx43 and Cx45: diversity of channels—diversity of electrical properties. In: Proceedings of the 2003 International Gap Junction Conference, Cambridge, UK, August 23–28, p 57
12. Elenes S, Martinez AD, Delmar M, Beyer EC, Moreno AP (2001) Heterotypic docking of Cx43 and Cx45 connexons blocks fast voltage gating of Cx43. Biophys J 81:1406–1418
13. Gros DB, Jongsma HJ (1996) Connexins in mammalian heart function. Bioessays 18:719–730
14. Halliday D, Dupont E, Coppen SR, Severs NJ (2003) Development of a cell model for functional and structural analysis of connexin co-expression: achieving homogeneous and inducible expression of multiple connexins in stable transfectants. Cell Commun Adhes 10:1–7
15. Harris AL (2001) Emerging issues of connexin channels: biophysics fills the gap. Q Rev Biophys 34:325–472
16. He DS, Jiang JX, Taffet SM, Burt JM (1999) Formation of heteromeric gap junction channels by connexins 40 and 43 in vascular smooth muscle cells. Proc Natl Acad Sci USA 96:6495–6500
17. Kanter HL, Laing JG, Beau SL, Beyer EC, Saffitz JE (1993) Distinct patterns of connexin expression in canine Purkinje fibers and ventricular muscle. Circ Res 72:1124–1131
18. Kanter HL, Laing JG, Beyer EC, Green KG, Saffitz JE (1993) Multiple connexins colocalize in canine ventricular myocyte gap junctions. Circ Res 73:344–350
19. Kistler J, Lin JS, Bond J, Green C, Eckert R, Merriman R, Tunstall M, Donaldson P (1999) Connexins in the lens: are they to blame in diabetic cataractogenesis? In: Gap junction-mediated intercellular signalling in health and disease (Novartis Foundation Symposium series, Vol. 219). Wiley, Chichester, pp 97–108
20. Kléber AG, Rudy Y (2004) Basic mechanisms of cardiac impulse propagation and associated arrhythmias. Physiol Rev 84:431–488
21. Lee MJ, Rhee SK (1998) Heteromeric gap junction channels in rat hepatocytes in which the expression of connexin26 is induced. Mol Cells 8:295–300
22. Moreno AP, Fishman GI, Beyer EC, Spray DC (1995) Voltage dependent gating and single channels analysis of heterotypic gap junction channels formed of Cx45 and Cx43. Progr Cell Res 4:405–408
23. Polontchouk, LD, Valiunas V, Haefliger J-A, Eppenberger HM, Weingart R (2002) Expression and regulation of connexins in cultured ventricular myocytes isolated from adult rat hearts. Pflugers Arch 443:676–689
24. Severs NJ (1999) Cardiovascular disease. In: Gap Junction-mediated intercellular signalling in health and disease (Novartis Foundation Symposium series, Vol. 219). Wiley, Chichester, pp 188–210
25. Steiner E, Ebihara L (1996) Functional characterization of canine connexin45. J Membr Biol 150:153–161
26. Trexler EB, Bennett, MVL, Bargiello TA, Verselis VK (1996) Voltage gating and permeation in a gap junction hemichannel. Proc Natl Acad Sci USA 93:5836–5841
27. Valiunas V (2002) Biophysical properties of connexin-45 gap junction hemichannels studied in vertebrate cells. J Gen Physiol 119:147–164
28. Valiunas V, Bukauskas FF, Weingart R (1997) Conductances and selective permeability of connexin43 gap junction channels examined in neonatal rat heart cells. Circ Res 80:708–719
29. Valiunas V, Manthey D, Vogel R, Willecke K, Weingart R (1999) Biophysical properties of mouse connexin30 gap junction channels studied in transfected human HeLa cells. J Physiol (Lond) 519:631–644
30. Valiunas V, Weingart R (2000) Electrical properties of gap junction hemichannels identified in transfected HeLa cells. Pflugers Arch 440:366–379
31. Valiunas V, Weingart R, Brink PR (2000) Formation of heterotypic gap junction channels by connexins 40 and 43. Circ Res 86:E42–E49
32. Valiunas V, Gemel J, Brink PR, Beyer EC (2001) Gap junction channels formed by coexpressed connexin40 and connexin43. Am J Physiol 281: H1675–H1689
33. Van Rijen HVM, Wilders R, Van Ginneken ACG, Jongsma HJ (1998) Quantitative analysis of dual whole-cell voltage-clamp determination of gap junctional conductance. Pflugers Arch 436:141–151
34. Van Veen AA, van Rijen HV, Opthof T (2001) Cardiac gap junction channels: modulation of expression and channel properties. Cardiovasc Res 51:217–229
35. Vogel R, Weingart R (1998) Mathematical model of vertebrate gap junctions derived from electrical measurements on homotypic and heterotypic channels. J Physiol (Lond) 510:177–189
36. Wang XG, Peracchia C (1998) Chemical gating of heteromeric and heterotypic gap junction channels. J Membr Biol 1998 162:169–176
37. Willecke K, Eiberger J, Degen J, Eckardt D, Romualdi A, Guldenagel M, Deutsch U, Sohl G (2002) Structural and functional diversity of connexin genes in the mouse and human genome. Biol Chem 383:725–737